IEEE Access
Multidisciplinary | Rapid Review | Open Access Journal

Received June 29, 2018, accepted August 7, 2018, date of publication August 13, 2018, date of current version September 5, 2018.

*Digital Object Identifier 10.1109/ACCESS.2018.2864999*

# A Crossed DD Geometry and Its Double-Coil Excitation Method for Electric Vehicle Dynamic Wireless Charging Systems

**LIJUAN XIANG, XIAOYU LI, JINDONG TIAN, AND YONG TIAN**

Key Laboratory of Optoelectronic Devices and Systems of Ministry of Education and Guangdong Province, College of Optoelectronic Engineering, Shenzhen University, Shenzhen 518060, China

Corresponding author: Yong Tian (ytian@szu.edu.cn)

This work was supported by the Science and Technology Plan Project of Shenzhen under Grant JCYJ20170412110241478.

**ABSTRACT** Dynamic wireless charging technology can supply power for electric vehicle (EV) while it is in-motion. However, the system output stability is heavily influenced by the mutual inductance variation of the magnetic coupler, which is a major drawback of the EV dynamic wireless power transfer (EV-DWPT). This paper focuses on the primary coil design and its activating method. First, the LCC compensation network was adopted in both primary side and pick-up side of the system to achieve the constant primary current characteristic. Subsequently, a double-coil excitation method with the crossed-DD coil structure was proposed, which specifically concentrates on the feature of the dynamic mutual inductance. Simulation studies were carried out to prove the effectiveness of the proposed system. An EV-DWPT system prototype was performed to further verify the theoretical and simulation results.

**INDEX TERMS** Dynamic wireless charging, electric vehicle, magnetic coupler, coil excitation.

## I. INTRODUCTION

Wireless Power Transfer (WPT) system can transfer the power from a power source to electrical equipment without the usage of wires or cables. There are different WPT approaches, such as inductive coupling, capacitive coupling, magnetic resonant coupling, and microwaves. In recent decades, WPT technology has been used extensively to supply power to household appliances, means of transportation, biological implants etc. [1]–[3]. A large number of research has been focused on the power transfer efficiency, system stability, misalignment tolerance, transmission distance, and circuit optimization of the WPT system [4]–[6].

Due to issues related to environment pollution and fossil energy crisis, the electric vehicles (EVs) have been widely developed around the world. The foremost existing charging infrastructures for EVs are conductive chargers. This kind of wired solution requires human involvement, which needs tediously long and heavy wires to connect the EV and the charger. WPT technology offers an alternative solution for charging the EVs in a contact-free manner. This technology not only effectively overcomes the shortcomings of the existing wired charging, but also is more convenient for automatic parking and other related frontier vehicle technologies. Furthermore, it complies with EVs' future development tendency. As a result, WPT technology in EV application has become an important research field, for both research groups and business enterprises globally [7]–[9]. For the EV application, WPT technology can be divided into two categories based on the EV's operation, namely EV Stationary Wireless Power Transfer (EV-SWPT) and EV Dynamic Wireless Power Transfer (EV-DWPT), as shown in Fig. 1.

(a) (b)

**FIGURE 1.** Two different wireless charging methods for EV. (a) EV-SWPT system. (b) EV-DWPT system.

Magnetic coupler is a key part for an EV-SWPT system, and it consists of a primary transmitter coil embedded in the charging station or home parking ground, and a pick-up coil installed underside the EV. EV-SWPT technology can handle issues related to the convenience and automation of EVs' charging. Studies have been investigated in the EV-SWPT

application, including improvements of efficiency [10], misalignment [11], design of the magnetic coupler structure [12], and power flow control [13]. Compared to the EV-SWPT, EV-DWPT may potentially eliminate existed challenges associated with range anxiety and bulky batteries.

An EV-DWPT system, in which a pick-up coil is embedded under the EV, and a series of coils/pads or a long track coil are installed on the roadway can wirelessly supply electrical energy to a moving EV in real-time. As shown in Fig. 2, there are $n$ primary devices, each of which is comprised of one inverter, one resonant network, and one primary coil. All primary devices, which are paralleled to each other are connected to the Grid. The secondary side is made up of the rectifier, the resonant compensation network, and the receiver coil. The EV receives the power from the primary coils sequentially when it's in motion. The coils are dynamically switched on or off according to the EV position.

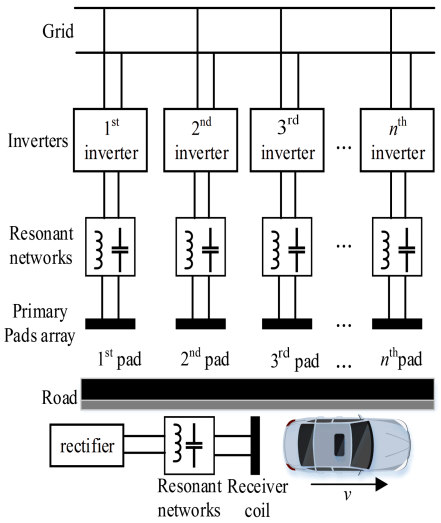


**FIGURE 2.** EV-DWPT system.

Bloger [14] developed an 8 kW EV-DWPT system in 1979, which opened up the research of this technology. In 1997, with cooperation from the University of Auckland, Wampfler AG realized a fast charging DWPT system with the output power of 30 kW and a charging time of only 2 to 3 minutes. Korea Advanced Institute of Science and Technology (KAIST) began to investigate the EV-DWPT since 2009 [15], and they have proposed a 5$^{th}$ generation prototype, considering the construction cost, magnetic coupler, and parameter optimization. The maximum output power reached to 25 kW, and the efficiency was about 80%. Oak National Laboratory developed an EV-DWPT system using coil array, and achieved lower EMC (Electro Magnetic Compatibility) and EMF (Electric and Magnetic Fields) values [16]. Li and Mi [17] developed a 1-MW DWPT system for the high-speed train, which consists of a 128 m long transmitter and four pickups. The measured efficiency at 818 kW output power point for 5 cm air gap was 82.7%. Li *et al.* [18] proposed a double-sided LCC compensation network and its tuning method. Besides, a 7.7 kW EV-DWPT system with 96% efficiency was conducted. Although a considerable number of works have been focused on the high-level output power, resonant compensation topologies, and transmitter coil design etc., the output power stability caused by the transmitter coil switching needs to be further investigated.

Considering previous needs and motivations, this paper extends and develops the work presented in [19]. The objective of this paper is to analyze performance of the EV-DWPT system with crossed DD coils and double-coil excitation strategy based on the previous work.

This paper is organized as follows. In Section 2, the circuit topology of the system is analyzed and the double-side LCC resonant networks are introduced. In Section 3, the Crossed DD coil geometry with double-coil excitation strategy is proposed to reduce fluctuations of the mutual inductance variation, so as to improve the system output stability. In Section 4, the simulation and experimental results are presented and discussed. Finally, the paper is concluded in Section 5.

## II. CIRCUIT TOPOLOGY ANALYSIS

The LCC resonant network has been widely used in EV-SWPT and EV-DWPT systems owing to its outstanding performance [20]. Firstly, compared to the traditional LC type, only EV consumes the active power in the LCC EV-DWPT system. Moreover, the current in the primary-side coil is independent of the load condition. Besides, the LCC resonant network has been one of the normalized candidates for an EV-SWPT system with the development of SAE 2954, ISO 19363, and IEC 61980. The equivalent circuit of LCC-LCC WPT system is shown in Fig. 3. $U_{in}$ represents the voltage input of the inverter, $U_{AB}$ and $U_{ab}$ represent the input and output voltage of the LCC-LCC resonant network, respectively. $L_{fp}$, $L_{fs}$, $C_{f1}$, $C_{f2}$, $C_p$, and $C_s$ are the compensation inductors and capacitors. $I_{fp}$ is the input current of primary resonant network and $I_{fs}$ is the output current of secondary resonant network, $I_p$ and $I_s$ are the currents of the transmitter coil and receiver coil, respectively. $L_p$ and $L_s$ are the inductive impedances of the transmitter coil and receiver coil, respectively. $M$ is the mutual inductance of $L_p$ and $L_s$. $R_L$ is the resistance of the load, $I_R$ and $U_R$ separately represent the current and voltage of the load $R_L$.

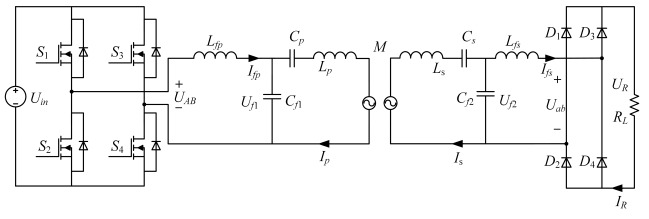


**FIGURE 3.** WPT system with double-side LCC resonant networks.

To simplify the equation derivations, the resistance of all the compensation inductors and capacitors are ignored, and only the fundamental harmonic is considered herein. Based on the Reflected Impedance Theory as well as Kirchhoff's

**TABLE 1. Simulation parameters.**

| Para. | Value | Para. | Value | Para. | Value | Range |
|---|---|---|---|---|---|---|
| $U_{AB}$ | 400V | $R_{Lp}$ | 0.1Ω | $M$ | 12μH | [1,30]μH |
| $L_p$ | 115.22μH | $R_{Ls}$ | 0.05Ω | $f$ | 85kHz | [79,90]kHz |
| $L_s$ | 116.26μH | | | $R_L$ | 25Ω | [20,30]Ω |

Laws in Circuit Analysis, currents and voltages on both sides can be expressed as:

$$I_{fp} = \frac{(\omega^2(M^2R_L + L_{fs}^2R_{Lp}) + R_LR_{Lp}R_{Ls})U_{AB}}{\omega^2L_{fp}^2(\omega^2L_{fs}^2 + R_LR_{Ls})} \quad (1)$$

$$I_p = \frac{U_{AB}}{\omega_0 L_{fp}} \quad (2)$$

$$I_s = \frac{U_{AB}MR_L}{L_{fp}\left(\omega_0^2L_{fs}^2 + R_{Ls}R_L\right)} \quad (3)$$

$$U_R = \frac{\omega_0 U_{AB}MR_LL_{fs}}{L_{fp}\left(\omega_0^2L_{fs}^2 + R_{Ls}R_L\right)} \quad (4)$$

Equation (2) indicates that the transmitter current $I_p$ is independent of the mutual inductance $M$ and the load $R_L$. Consequently, the system performs the constant transmitter current characteristic, which can avoid the primary current from increasing sharply when EV moves to next primary coil. This is really important for the dynamic wireless charging for EV.

Furthermore, the system output power and efficiency can be obtained as:

$$P_{out} = \frac{\omega_0^2M^2U_{AB}^2L_{fs}^2R_L}{L_{fp}^2\left(R_{Ls}R_L + \omega_0^2L_{fs}^2\right)^2} \quad (5)$$

$$\eta = \frac{\omega_0^4M^2R_LL_{fs}^2}{\left(\omega_0^2M^2R_L + R_{Lp}\omega_0^2L_{fs}^2 + R_{Lp}R_{Ls}R_L\right)\left(R_{Ls}R_L + \omega_0^2L_{fs}^2\right)} \quad (6)$$

According to Equations (5) and (6), the output power and efficiency are related to the series inductance $L_{fp}$ and $L_{fs}$, which should be considered as optimization parameters in the EV-DWPT system. To analyze the relationship among these three variables ($M$, $f$, and $R_L$) and the output power and efficiency, simulations with parameters in Table 1 had been carried out.

Fig. 4 presents the system output power and efficiency considering operation frequency $f$, mutual inductance $M$ and load resistance $R_L$. It can be seen that the output power and the efficiency are mainly influenced by the mutual inductance $M$. Fig. 4(a) and Fig. 4(b) show that $M$ has a strong and positive correlation with the output power, which means $M$ should be designed to be large enough in order to achieve the acceptable output power. Meanwhile, according to Fig. 4(c) and Fig. 4(d), it is clear that with the increase

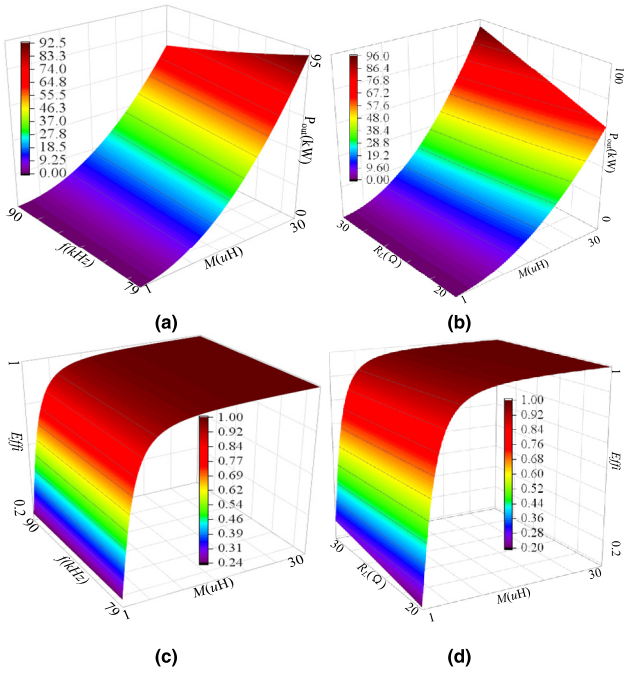


**FIGURE 4. The relationship among the output characteristics and the three main system electrical parameters: (a) Output power curved surface under different *M* and *f*; (b) Output power curved surface under different *M* and $R_L$; (c) Efficiency curved surface under different *M* and *f*; (d) Efficiency curved surface under different *M* and $R_L$.**

of $M$, the efficiency presents paraboloid characteristics. The efficiency firstly increases in the range of $M = [1, 15]$ $\mu$H, then remains steady. Taking into account, comprehensively including the output power and efficiency, we should design a reasonable range of $M$.

## III. PRIMARY COILS EXCITATION METHOD

The primary coils and secondary coil make up the magnetic coupler. To improve the dynamic performance of the magnetic coupler in the EV-DWPT system, the primary coils should be designed well and should achieve high output power, high efficiency, and low EMF. Based on the coil structure types, the magnetic coupler for the EV-DWPT system can be classified into two categories. One is the long rail, and the other is coils array. Long rail suffers from the large EMI and low efficiency issues, so the coils array is more attractive. Circular coils and Double D (DD) coils are the two commonly used coil types (segmented rails). Compared to the Circular coils, the DD coils have a higher coupling coefficient and a higher offset tolerance. However, it still has such a feature that the mutual inductance drops dramatically when EV moves into the switching area, making EVs fail to achieve enough power. In order to solve these problems, the Crossed DD primary coils geometry and its double-coil excitation strategy are investigated in this paper. The Crossed DD magnetic coupler and pick-up coil, as well as their dimensions are shown in Fig. 5. Two coils with a crossed area of half size of

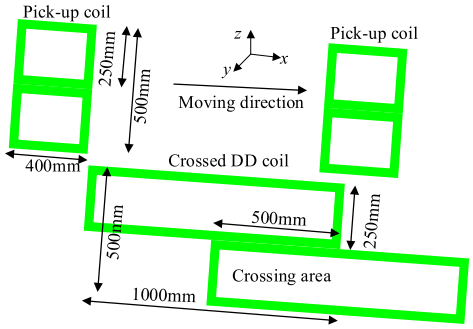


**FIGURE 5.** Magnetic coupler configuration with Crossed DD coil.

the coil length consist a crossed DD primary coil pair, which is activated by a primary inverter.

Fig. 6 presents two different kinds of coil excitation strategies, namely single-coil excitation and double-coil excitation. Different color coils and relative mutual inductance curves are given in this figure to make them be presented more clearly. When EV moves along with each primary coils pair, the mutual inductance $M$ firstly increases from a value approximating to zero to a maximum value, then drops to nearly zero with a symmetric opposite tendency. At each switching point, the working coil is changed, which means that different corresponding coils are turned OFF or ON at this particular time. The conventional single-coil excitation method is shown in Fig. 6(a). It can be seen that the mutual inductance varies from 6 $\mu$H to 12 $\mu$H. As discussed in the above section, mutual inductance is one of the most critical electrical parameters for the EV-DWPT system to guarantee the output power stability. Therefore, the double-coil excitation method is proposed in this paper, which is shown in Fig. 6(b). In Fig .6(b), it can be seen that the mutual inductance varies in the range of [12, 12.4] $\mu$H.

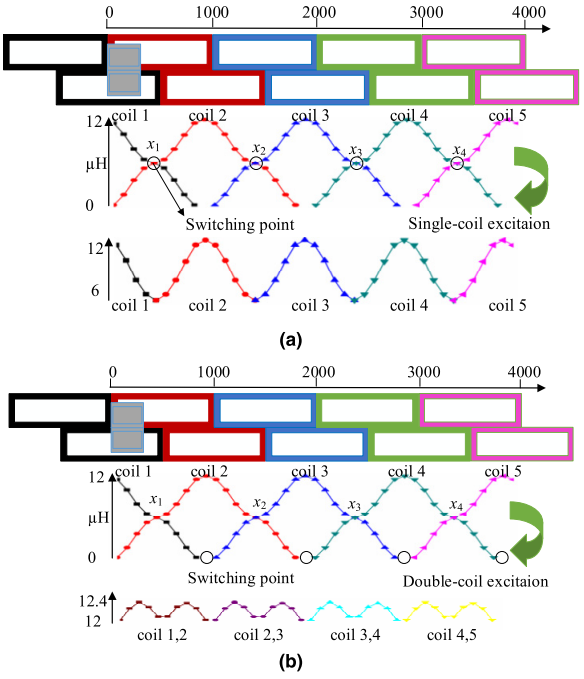


**FIGURE 6.** Two different coil excitation methods. (a) single-coil excitation method and (b) double-coil excitation method.

In Fig. 6, 'coil 1, 2' means that the 1st and 2nd coils are turned ON (excited mode) to supply power to the EV at that period, meanwhile, other coils are turned OFF (stand-by mode). When EV reaches the switching point $x_1$, the 1st coil is switched to stand-by mode, while the 3rd coil is switched to excited mode, and the 2nd coil is still kept in its original operating mode.

The equivalent schematic of the EV-DWPT system using the double-coil excitation method is shown in Fig. 7, where $I_{p1}$ and $I_{p2}$ represent the transmitter currents in the first and second primary coils respectively, $I_{fp1}$ and $I_{fp2}$ represent the total currents of two primary inverters, $I_s$ represents the receiver current of the pick-up coil, $M_{1s}$ and $M_{2s}$ represent the mutual inductance between the first primary and second primary coil and pick-up coil, respectively. $M_{12}$ represents the mutual inductance between the two adjacent primary coils.

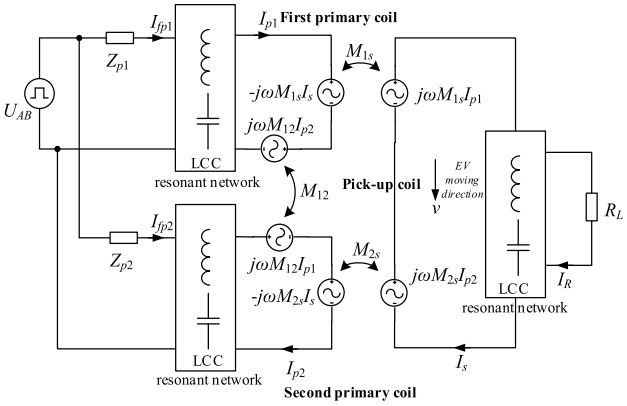


**FIGURE 7.** Equivalent circuit of EV-DWPT system using double-coil excitation method.

As analyzed in our previous work [19], the adjacent mutual inductances can be ignored in the proposed EV-DWPT. Consequently, some relevant currents and voltages can be derived as:

$$\begin{cases} I_{fp1} = \dfrac{(\omega^2(M_{1s}(M_{1s}+M_{2s})R_L + L_{fs}^2 R_{Lp}) + R_L R_{Lp} R_{Ls})U_{AB}}{\omega^2 L_{fp}^2(\omega^2 L_{fs}^2 + R_L R_{Ls})} \\ I_{fp2} = \dfrac{(\omega^2(M_{2s}(M_{1s}+M_{2s})R_L + L_{fs}^2 R_{Lp}) + R_L R_{Lp} R_{Ls})U_{AB}}{\omega^2 L_{fp}^2(\omega^2 L_{fs}^2 + R_L R_{Ls})} \\ I_{p1} = \dfrac{U_{AB}}{\omega L_{fp}} \\ I_{p2} = \dfrac{U_{AB}}{\omega L_{fp}} \\ I_s = \dfrac{U_{AB} R_L (M_{1s} + M_{2s})}{L_{fp}(\omega^2 L_{fs}^2 + R_L R_{Ls})} \\ I_R = \dfrac{\omega L_{fs} U_{AB}(M_{1s} + M_{2s})}{L_{fp}(\omega^2 L_{fs}^2 + R_L R_{Ls})} \end{cases} \tag{7}$$

More details regarding to the inverter topology used in this EV-DWPT system can be found in [21]. In order to control the output voltage and power, two primary resonant network input currents, $I_{fp1}$ and $I_{fp2}$ should be in the same phase. The angle of these two currents with input voltage $U_{AB}$ can be expressed as:

$$\theta_{IUin-x} = \arctan\left(\frac{\mathrm{Im}\left(Z_{px}\right)}{\mathrm{Re}\left(Z_{px}\right)}\right) \tag{8}$$

where $Z_{px}$ ($x = 1, 2$) represents the total primary reflected impedance.

For LCC-LCC resonant type, $Z_{px}$ can be derived as:

$$Z_{px} = j\omega L_{fp} + \frac{1}{j\omega C_{f1} + \frac{1}{\frac{1}{j\omega C_p} + j\omega L_p + Z_r}} \tag{9}$$

where,

$$Z_r = \frac{\omega^2 M^2}{j\omega L_s + \frac{1}{j\omega C_s} + \frac{1}{j\omega C_{f2} + \frac{1}{j\omega L_{fs} + R_L}}} \tag{10}$$

When the system operates in resonant frequency, $Z_p$ can be written as,

$$Z_p = \frac{\omega_0^2 L_{fp}^2 L_{fs}^2}{M^2 R_L} \tag{11}$$

The value of the phase angle is fixed under this condition. Fig. 8 shows the relationship between the phase angle and the operating frequency when the system does not work in resonant frequency.

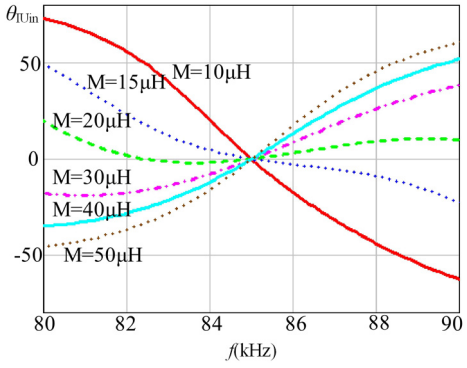


**FIGURE 8.** Phase angle variation curves with different frequency and mutual inductance values.

In Fig. 8, it is clear that the phase angle is independent of the mutual inductance when operating frequency is equal to the resonant frequency. On the contrary, the phase angle fluctuates with $M$ when the system operates at non-resonant frequency point. At the switching points using the double-coil excitation method, because the $M_{1s}$ and $M_{2s}$ are not the same, the phase angle cannot be of the same value. Therefore, in order to transfer the power stably, the system should work in the resonant frequency, and the total output current of the inverter $I_{fp}$ can be expressed as:

$$I_{fp} = \frac{(\omega^2((M_{1s} + M_{2s})^2 R_L + 2L_{fs}^2 R_{Lp}) + 2R_L R_{Lp} R_{Ls})U_{AB}}{\omega^2 L_{fp}^2(\omega^2 L_{fs}^2 + R_L R_{Ls})} \tag{12}$$

The total output power $P_{out}$ can be obtained as:

$$P_{out} = I_R^2 \cdot R_L = \frac{\omega^2 L_{fs}^2 U_{AB}^2 (M_{1s} + M_{2s})^2 R_L}{L_{fp}^2(\omega^2 L_{fs}^2 + R_L R_{Ls})^2} \tag{13}$$

And the output power divided by the total consuming power yields the efficiency $\eta$ (14), as shown at the bottom of the next page.

Using the above simulative mutual inductance values shown in Fig. 6, the dynamic variation curves of primary inverter output current, system output power, and the efficiency can be drawn as shown in Fig. 9.

In Fig. 9, the black solid curves represent results of the proposed double-coil excitation method, while the red dashed lines represent that of the conventional single coil excitation method. It is indicated that compared to the single-coil excitation method, the EV-DWPT system with the double-coil excitation method, performs more stable output power with higher efficiency.

## IV. SIMULATIONS AND EXPERIMENTAL RESULTS

In order to verify the feasibility of the proposed EV-DWPT system, simulations are conducted in this Section. On the one hand, using the Ansys Maxwell software, the magnetic flux in one switching point with different coil geometries and coil excitation methods are compared to each other. On the other hand, the simulative analysis of the proposed EV-DWPT system was performed using the ANSYS Simplorer and Maxwell co-simulation method.

Fig. 10 shows the magnetic flux distributions of the pick-up coil at the switching point using different coil configurations and excitation methods.

Fig. 10(a) and (b) reveal that compared to the conventional DD coil type, more magnetic flux can be obtained with the proposed Crossed DD coil geometry. Fig. 10(c) indicates that the double-coil excitation method produces greater magnetic flux through the pick-up coil, which means more energy could be transferred to the EV. Besides, the magnetic flux distribution is more uniform as using the proposed magnetic coupler design, including Crossed DD coil configuration and the double-coil excitation method.

Fig. 11 shows the compensation network current waveform in the primary side of the EV-DWPT system. The blue one represents the LCC resonant input current, which is injected to the first excitation coil, while the yellow one indicates that injected in the second excitation coil. Each waveform involves four stages, including stand-by, ascending working, descending working and stand-by, respectively. Furthermore, $I_{p2}$ lags behind $I_{p1}$ for the half of one working period.

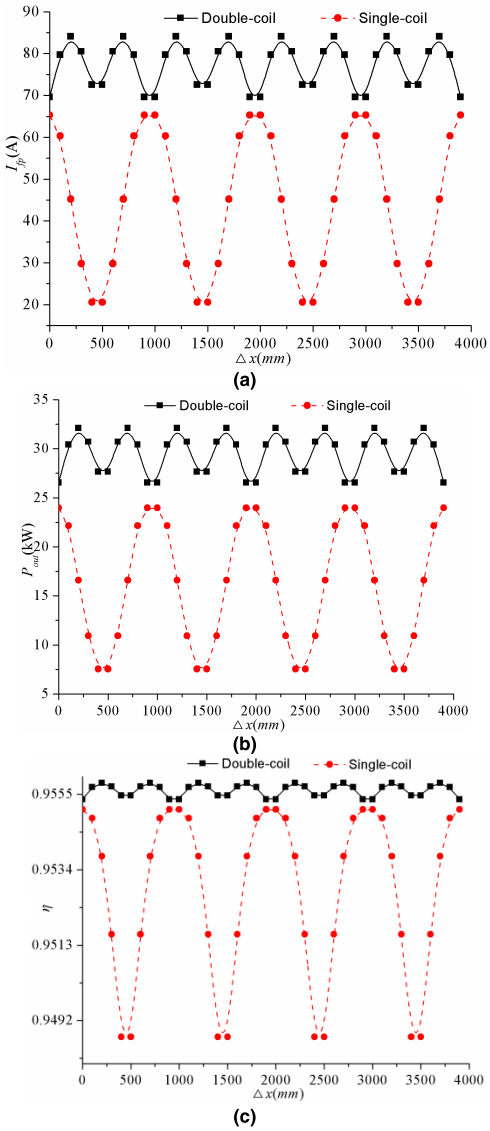


**FIGURE 9.** Variation curves when EV moves with different coil excitation methods. (a) the primary inverter input current; (b) the output power; (c) the efficiency.

Fig. 12 shows the transmitter currents in the two excitation coils. The purple waveform represents the first excitation coil current in double-coil strategy, while the yellow one represents the second coil current. It can be seen that the transmitter current value remains constant when the coil is working, indicating that the EV-DWPT system with the LCC-LCC resonant network has the constant primary current characteristic, which is benefit for system controlling and overcurrent protection.

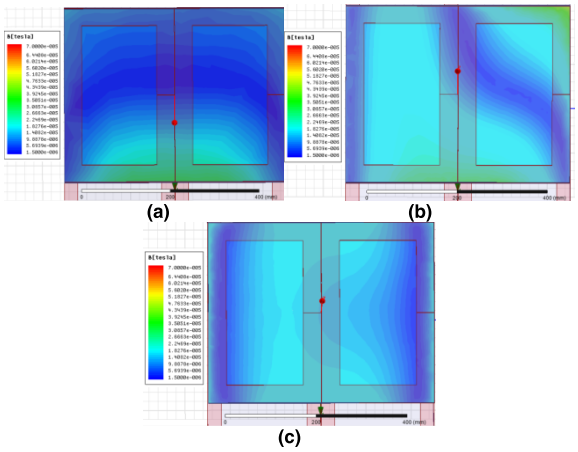


**FIGURE 10.** Magnetic B distribution using different coil configurations and excitation methods. (a) DD coil type (b) Crossed DD type with single-coil excitation method. (c) Crossed DD type with double-coil excitation method.

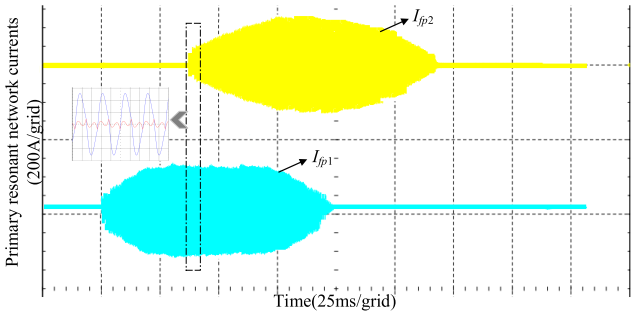


**FIGURE 11.** Input current waveform of the primary LCC resonant networks.

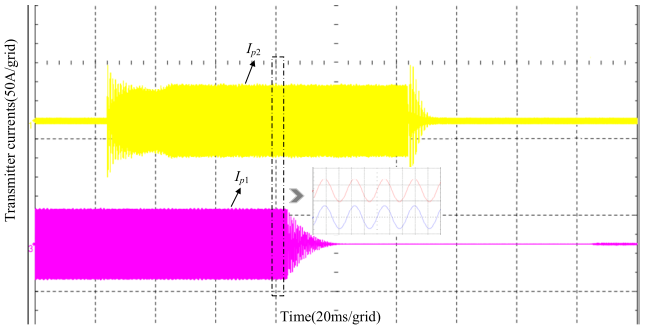


**FIGURE 12.** The transmitter current waveform of two primary coils.

To further evaluate the advantages of the proposed system, a 50 meters EV-DWPT system prototype was constructed as shown in Fig. 13, which included the conventional DD and Crossed DD coil types.

$$\eta = \frac{\omega^4 L_{fs}^2 (M_{1s} + M_{2s})^2 R_L}{(\omega^2 L_{fs}^2 + R_L R_{Ls})(\omega^2 (M_{1s} + M_{2s})^2 R_L + 2R_{Lp}(\omega^2 L_{f2}^2 + R_L R_{Ls}))} \tag{14}$$

**FIGURE 13.** EV-DWPT system prototype.

Figs. 14 and 15 show the current and voltage waveforms in both primary and secondary circuits during the charging process. The blue waveforms represent the voltages, and the red ones are the current waveforms. The output power values for the two coil geometries are assumed to be the same.

As seen in the Fig. 14 (a) - (c), in the non-switching area, the output power was set as 4.07 kW (shown in the Fig. 14(c), the output voltage was 251 V, the output current was 16.2A). For the Crossed DD type, as shown in Fig. 14(a), the input voltage effective value $U_{AB}$ multiplied by the input current effective value $I_{fp}$ equals 5.13 kVA (the voltage was 421 V, and the current was 12.2 A). For the DD type, as shown in Fig. 14(b), the product of the input voltage effective value and input current effective value was 5.36 kVA (the voltage was 432 V, and the current was 12.4 A).

Because phase difference exists between the input voltage and current of the resonant network, product of these two values does not yield the primary input power. In order to get the real values of the power, Power Analyzer was adopted during the experiments. For the Crossed DD type, the input power was 4.57 kW (the voltage was 219 V, and the current was 20.87 A), the system efficiency was 89.2%. For the DD type, the input power was 4.60 kW (the voltage was 220 V, and the current was 20.92 A), the system efficiency was 88.5%. It is indicated that, for these two different coil geometries, the system performs the similar characteristics when the output power values were the same.

Furthermore, the system characteristics in the switching area were also analyzed. The output power values for the two different coil geometries are still the same (3.79 kW). The waveforms are given in Fig. 15. It can be seen that, in the switching point, the system efficiency using the proposed Crossed DD geometry was 88.7%, while the value with the conventional DD type was 81.2%. In other words, the crossed DD geometry with double-coil excitation can significantly improve the system efficiency at switching point by 7.5% compared to the conventional DD coils.

Table 2 summarizes the experimental results considering the switching and non-switching areas. With all of the above experimental results, it can be concluded that compared to the DD coil, the Crossed DD geometry has a higher efficiency when the output power values are set to be the same,

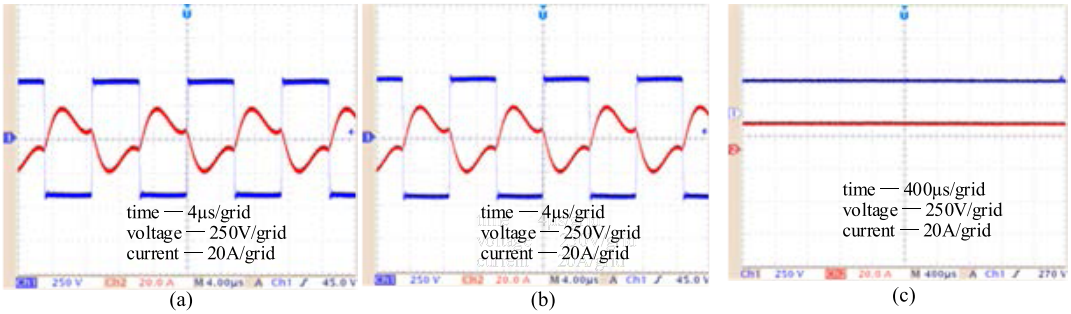


**FIGURE 14.** The waveforms in one non-switching point. (a) the primary LCC resonant network current waveform with the Crossed DD coils; (b) the primary LCC resonant network current waveform with the DD coils; (c) voltage and current of the load.

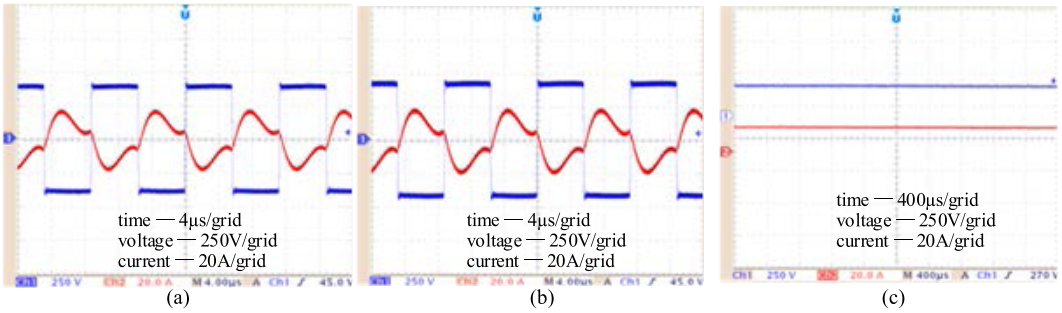


**FIGURE 15.** The waveforms in one switching point. (a) the primary LCC resonant network current waveform with the Crossed DD type; (b) the primary LCC resonant network current waveform with the DD type; (c) voltage and current of the load.

**TABLE 2. Experimental results.**

| Para. | Non-switching point | | Switching point | |
|---|---|---|---|---|
| | Crossed DD | DD type | Crossed DD | DD type |
| $I_{fp}$(A) | 12.2 | 12.4 | 11.4 | 12.8 |
| $U_{AB}$(V) | 421 | 432 | 393 | 437 |
| $I_{fs}$(A) | 17.5 | 17.5 | 16.5 | 16.5 |
| $U_{ab}$(V) | 276 | 276 | 260 | 260 |
| $I_R$(A) | 16.2 | 16.2 | 15.8 | 15.8 |
| $U_{RL}$(V) | 251 | 251 | 240 | 240 |
| $P_{out}$(kW) | 4.07 | 4.07 | 3.79 | 3.79 |
| $P_{\text{in}}$(kW) | 4.57 | 4.60 | 4.28 | 4.67 |
| $\eta$ | 89.2% | 88.5% | 88.7% | 81.2% |

especially at the switching point. Besides, for the crossed DD geometry with double-coil excitation, the system efficiency is nearly invariable regardless of the EV position. However, for the conventional DD coils, the efficiency is greatly decreased when the pick-up coil moves from the non-switching area to the switching area.

## V. CONCLUSIONS

Stable output is a greatly critical issue for the EV-DWPT system. However, the output of a practical EV-DWPT system is influenced by factors, such as mutual inductance, resonant compensation topology, and load resistance. In this paper, the double-side LCC resonant network was adopted to obtain the constant primary current characteristic. A crossed DD coil geometry with double-coil excitation method was proposed to reduce the mutual inductance fluctuation, so as to guarantee the output stability, including the output power and the efficiency. Simulations and experimental results revealed that the system efficiency with the crossed DD geometry and double-coil excitation is nearly invariable (from 89.2% to 88.7%) regardless of the EV position, while that with the conventional DD coils is greatly decreased (from 88.5% to 81.2%) when the pick-up coil moves from the non-switching area to the switching area. It is concluded that the proposed crossed DD geometry with double-coil excitation can greatly improve the system output stability compared to the conventional DD geometry.

## REFERENCES


[1] Y. D. Chung, C. Y. Lee, D. W. Kim, H. Kang, Y. G. Park, and Y. S. Yoon, "Conceptual design and operating characteristics of multi-resonance antennas in the wireless power charging system for superconducting MAGLEV train," *IEEE Trans. Appl. Supercond.*, vol. 27, no. 4, Jun. 2017, Art. no. 3601805.

[2] S. Y. R. Hui, "Technical and safety challenges in emerging trends of near-field wireless power transfer industrial guidelines," *IEEE Electromagn. Compat. Mag.*, vol. 7, no. 1, pp. 78–86, 1st Quart., 2018.

[3] T. Kan, R. Mai, P. P. Mercier, and C. C. Mi, "Design and analysis of a three-phase wireless charging system for lightweight autonomous underwater vehicles," *IEEE Trans. Power Electron.*, vol. 33, no. 8, pp. 6622–6632, Aug. 2018.

[4] Y. Liu, R. Mai, D. Liu, Y. Li, and Z. He, "Efficiency optimization for wireless dynamic charging system with overlapped DD coil arrays," *IEEE Trans. Power Electron.*, vol. 33, no. 4, pp. 2832–2846, Apr. 2018.

[5] S. Samanta, A. K. Rathore, and D. J. Thrimawithana, "Analysis and design of current-fed half-bridge (C)(LC)–(LC) resonant topology for inductive wireless power transfer application," *IEEE Trans. Ind. Appl.*, vol. 53, no. 4, pp. 3917–3926, Jul./Aug. 2017.

[6] W. Shi, J. Deng, Z. Wang, and X. Cheng, "The start-up dynamic analysis and one cycle control-PD control combined strategy for primary-side controlled wireless power transfer system," *IEEE ACCESS*, vol. 6, pp. 14439–14450, 2018.

[7] A. Ahmad, M. S. Alam, and R. Chabaan, "A comprehensive review of wireless charging technologies for electric vehicles," *IEEE Trans. Transport. Electrific.*, vol. 4, no. 1, pp. 38–63, Mar. 2018.

[8] D. Patil, M. K. McDonough, J. M. Miller, B. Fahimi, and P. T. Balsara, "Wireless power transfer for vehicular applications: Overview and challenges," *IEEE Trans. Transport. Electrific.*, vol. 4, no. 1, pp. 3–37, Mar. 2018.

[9] C. Cai *et al.*, "Design and optimization of load-independent magnetic resonant wireless charging system for electric vehicles," *IEEE ACCESS*, vol. 6, pp. 17264–17274, 2018.

[10] Y.-C. Hsieh, Z.-R. Lin, M.-C. Chen, H.-C. Hsieh, Y.-C. Liu, and H.-J. Chiu, "High-efficiency wireless power transfer system for electric vehicle applications," *IEEE Trans. Circuits Syst. II, Exp. Briefs*, vol. 64, no. 8, pp. 942–946, Aug. 2017.

[11] L. Zhao, D. J. Thrimawithana, and U. K. Madawala, "Hybrid bidirectional wireless EV charging system tolerant to pad misalignment," *IEEE Trans. Ind. Electron.*, vol. 64, no. 9, pp. 7079–7086, Sep. 2017.

[12] Q. Zhu, Y. Zhang, Y. Guo, C. Liao, L. Wang, and L. Wang, "Null-coupled electromagnetic field canceling coil for wireless power transfer system," *IEEE Trans. Transport. Electrific.*, vol. 3, no. 2, pp. 464–473, Jun. 2017.

[13] J. M. Miller, O. C. Onar, and M. Chinthavali, "Primary-side power flow control of wireless power transfer for electric vehicle charging," *IEEE J. Emerg. Sel. Topics Power Electron.*, vol. 3, no. 1, pp. 147–162, Jan. 2014.

[14] J. G. Bolger, L. S. Ng, D. B. Turner, and R. I. Wallace, "Testing a prototype inductive power coupling for an electric highway system," in *Proc. IEEE Veh. Technol. Conf.*, Mar. 1979, pp. 48–56.

[15] C. C. Mi, G. Buja, S. Y. Choi, and C. T. Rim, "Modern advances in wireless power transfer systems for roadway powered electric vehicles," *IEEE Trans. Ind. Electron.*, vol. 63, no. 10, pp. 6533–6545, Oct. 2016.

[16] J. M. Miller, P. T. Jones, J.-M. Li, and O. C. Onar, "ORNL experience and challenges facing dynamic wireless power charging of EV's," *IEEE Circuits Syst. Mag.*, vol. 15, no. 2, pp. 40–53, 2nd Quart., 2015.

[17] S. Li and C. C. Mi, "Wireless power transfer for electric vehicle applications," *IEEE J. Emerg. Sel. Topics Power Electron.*, vol. 3, no. 1, pp. 4–17, Mar. 2015.

[18] S. Li, W. Li, J. Deng, T. D. Nguyen, and C. C. Mi, "A double-sided LCC compensation network and its tuning method for wireless power transfer," *IEEE Trans. Veh. Technol.*, vol. 64, no. 6, pp. 2261–2273, Jun. 2015.

[19] L. Xiang, Y. Sun, C. Tang, X. Dai, and C. Jiang, "Design of crossed DD coil for dynamic wireless charging of electric vehicles," in *Proc. IEEE PELS Workshop Emerg. Technol., Wireless Power Transf. (WoW)*, May 2017, pp. 343–347.

[20] C. Liao, J. Li, and S. Li, "Design of LCC impedance matching circuit for wireless power transfer system under rectifier load," *CPSS Trans. Power Electron. Appl.*, vol. 2, no. 3, pp. 237–245, 2017.

[21] L. Xiang, Y. Sun, Z. Ye, Z. Wang, and S. Zhou, "Combined primary coupler design and control for EV dynamic wireless charging system," in *Proc. IEEE PELS Workshop Emerg. Technol., Wireless Power Transf. (WoW)*, Oct. 2016, pp. 174–179.


**LIJUAN XIANG** received the B.S. degree in automation and the Ph.D. degree in control theory and control engineering from the College of Automation, Chongqing University, Chongqing, China, in 2012 and 2017, respectively.

From 2016 to 2017, she was a Joint Ph.D. Student with The Pennsylvania State University, State College, PA, USA, sponsored by the China Scholarship Council. She is currently a Post-Doctoral Researcher with the College of Optoelectronic Engineering, Shenzhen University, China. Her research interests include electromagnetic field modeling and simulation, control theory and application, and wireless power transfer.

**XIAOYU LI** received the B.S., M.S., and Ph.D. degrees in instrument science and technology from the Harbin Institute of Technology, Harbin, China, in 2011, 2013, and 2018, respectively.

From 2016 to 2017, he was a Visiting Scholar of electrical engineering with the Center for Automotive Research, The Ohio State University, Columbus, OH, USA. He is currently an Assistant Professor with the College of Optoelectronic Engineering, Shenzhen University. His research interests include battery *in situ* testing, state estimation, fault diagnosis, and wireless power transfer.

**JINDONG TIAN** received the B.S. degree in precision machinery, the M.S. degree in optical instrument, and the Ph.D. degree in optical engineering from Tianjin University, Tianjin, China, in 1995, 1998, and 2001, respectively.

From 2001 to 2002, he was a Post-Doctoral Researcher with the Department of Mechanical Engineering, The Hong Kong University of Science and Technology, China. He is currently a Professor with the College of Optoelectronic Engineering, Shenzhen University. His research interests include optical metrology, wireless power transfer, and lithium-ion battery management.

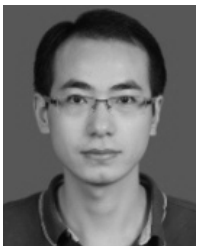

**YONG TIAN** received the B.S. degree in automation and the Ph.D. degree in control theory and control engineering from the College of Automation, Chongqing University, Chongqing, China, in 2008 and 2012, respectively.

From 2013 to 2015, he was a Post-Doctoral Researcher with the Department of Mechanical Engineering, Tsinghua University, China. He is currently an Assistant Professor with the College of Optoelectronic Engineering, Shenzhen University. His research interests include wireless power transfer, computational and artificial intelligence, and lithium-ion battery management.